ENGINEERING TRANSACTIONS • *Engng. Trans.* • **52**, 1-2, 37–55, 2004
Polish Academy of Sciences • Institute of Fundamental Technological Research
10.24423/engtrans.468.2004

VIBRO-IMPACT MOTION OF HEAVILY LOADED COMPACT HARD BODIES

Z. K o w a l s k a

Institute of Fundamental Technological Research, PAS
Świętokrzyska 21, 00-049 Warsaw
e-mail: Zofia.Kowalska@ippt.gov.pl

In the paper, the particular problems of modelling and simulation of dynamic unilateral contact of compact hard bodies are considered. Special attention is given to the rolling contact of bodies with irregular rolling surfaces. Due to inertia of the bodies and large but finite contact stiffness, contact vibrations arise and transient contact discontinuities may occur. In the developed algorithms, Hertzian model of contact is used within the elastic range. Two different quasi-static models of contact are used whenever during simulation the dynamic contact force exceeds its limiting value for the first plastic flow. The modelling problems considered herein are related mainly to the wheel/rail normal contact in rail transport. On the basis of simulations, plastic deformations resulting from free excessive vertical oscillations are proposed as one of the possible causes of rail and wheel corrugations.

Key words: vibro-impact motion, wheel/rail system

NOTATIONS

a	amplitude of a surface irregularity,
λ	wavelength of a periodic irregularity,
R	radius of the rolling body (wheel),
$y_r(x)$	profile of the foundation (rail),
$y_C(t)$	vertical position of the centre of the rolling body (wheel),
$y_C^k(x)$	vertical position of the centre of the wheel in constrained motion (the rigid wheel in contact with the rigid rail), also referred to as the rigid constraint,
V_t	constant rolling velocity (train speed), independent of vertical motion,
P	magnitude of the external load, i.e. vertical force acting on the moving mass,
m	moving mass, in particular cases the mass of the wheelset,
Y	uniaxial yield stress,
F	normal contact force,
F_Y	limiting normal force for elastic deformation by the Hertz theory,
δ	total indentation (relative approach),
δ_Y	limiting indentation for elastic deformation by the Hertz theory,

δ_r change in indentation during unloading,
δ_f final indentation, when the compressed bodies separate, $\delta_f = \delta_c - \delta_r$.
R_* the effective radius of contact; for two spheres of radius R_1 and R_2 it equals $R_* = R_1 R_2/(R_1 + R_2)$.

1. Introduction

The basic object of the simulation studies is a compact mass m pressed against the foundation of irregular surface by the external vertical force P (Fig. 1a). The mass is assumed to be rigid, only local contact compliance is taken into account. In the paper, the dynamics of such a system is discussed mainly in the context of the wheel/rail normal interaction. The compact mass m represents the so-called unsprung mass, in contrast to the sprung mass of the vehicle, which is dynamically isolated from the foundation by inertia of the unsprung mass and relatively soft springs of the vehicle suspension. The rolling unsprung mass is herein for simplicity referred to also as the wheel mass. It is worth to note, however, that the problems discussed in the paper are encountered in modelling, computer simulation and analysis of the unilateral contact between different other machine parts, for instance: a cam and a follower; a ball and its race in a rolling bearing; contacting gear teeth; an electrical brush and a commutator ring.

Irregularities on rolling (or sliding) surfaces are the source of complex excitation. In analogy to the simplest one-DOF mass-spring system, the excitation resembles the excitation by moving a spring base, but it also includes an additional parametric excitation due to variations in contact stiffness, caused by variations of curvature of irregularities at the contact point. The excitation may lead to transient discontinuities of contact, which are usually highly undesirable, especially in the presence of lateral forces.

The loss of contact of heavily loaded bodies is followed by impact with excessive contact forces and stresses. Therefore the problem arises of how to model elastic-plastic rolling contact with superimposed vertical vibro-impacts.

It is a common practice to model a normal wheel/rail contact by means of a Hertzian model, which is justified for smooth and regular surfaces of wheel and rail. Unavoidable irregularities may increase the transient normal forces by several times, up to the value much higher than the limiting force for the so-called first flow that takes place at the point below the surface, according to the Hertz theory and the von Mises yield criterion.

In the paper two models of elastic-plastic contact between a wheel and a rail are considered. The first model is based on Johnson's static model of elastic-plastic normal contact of spherical bodies. The second is a combination of Hertzian model in elastic range and a perfectly plastic model for the indentation greater than its limiting value for the first plastic flow. These two models are treated here as extreme models of elastic-plastic normal contact the properties

of which vary, depending on various factors like temperature, material properties and imperfections, additional tangential forces, etc.

The wheel/rail dynamic interaction is usually discussed in the context of noise generation and wear. Wear on rails and wheels is a very serious technical and economic problem. Both the wheel/rail dynamic interaction and the wear mechanisms are very complex. Field tests are difficult to be performed. All these factors make the problem very difficult to study and therefore many wear phenomena observed on wheels and rails are, to a large extent, still hypothetical [1]. Because of the importance and complexity of wear and noise generation in moving contact, the literature on various related problems is enormous. Critical analysis of the whole literature would be a great effort and is beyond the scope of this paper. The reference section provides mainly the fundamental literature on Hertzian [3, 8] and Johnson's model [6, 7] of solid bodies contact. These models were converted into the computer models and used in the simulation studies. Amongst other references it is worth to mention the paper by KNOTHE [5] which contains an excellent bibliography of many related papers and the paper by IGELAND [4], where the notion of the effective irregularity is introduced. The effective irregularity is analogous to the notion of the rigid constraint that is used herein, but they are not entirely equivalent.

The aim is to explore some aspects of the wheel/rail dynamic interaction which are usually neglected, namely the influence of contact discontinuities and plastic deformations on dynamic behavior of the system. Usually these two factors are neglected under an arbitrary assumption that inertia forces excited by realistic irregularities cannot override relatively high static external load which presses the wheel against the rail. A very simple model is used herein, however it helps to understand the main dynamic features of the system under consideration.

The tendency of the moving mass, representing the wheel, to bounce off the irregular surface of the foundation increases when the external static load decreases. Therefore transient contact discontinuities and impacts in the wheel/rail system seem to play a greater role in wear and noise generation in light rail systems and passenger high speed railways than in heavy railways, where the axle loads are much higher. The European maximum axle load for traditional railways is 22.5 t.

The simulations show that an occurrence of the wheel/rail contact discontinuities and impacts depends very much on dynamical properties of the foundation. On the stiff concrete slab track of large dynamic inertia, impacts are more likely to occur and influence the whole dynamic behaviour. The stiff slab track is of our particular interests because our intention is to perform an introductory

simulation research aimed at formulation of the specifications for construction of special test site on a railway track, which would enable diagnostics of wheel faults and parametric identification of the wheels suspensions. The main features of slab track include: good precision of track lying, good control and stability of mechanical properties, which are advantageous in normal operation conditions, but absolutely necessary when measuring the wheel/rail interaction on a special test site for diagnostics and identification purposes.

Plastic deformations during transient vertical oscillations of the wheel induced by strong random excitation are proposed as one of possible explanations of rail corrugations. For example, a stone from a track ballast randomly located between a wheel and a rail may be, under certain conditions, an initial cause of few corrugations on the rail and/or the wheel tread, which in turn excite oscillations of the next wheel and thus the corrugation process develops along the rail and wheel circumference.

All simulation results presented in this paper are obtained with the author's own computer programs. Numerical problems of simulation are not discussed herein, however it is worth to mention that in the case of systems under consideration, time histories obtained via simulation are very sensitive to errors in times at which the bodies loose contact or come into contact. Moreover, sliding motion along the constraints cannot be excluded and this may lead to the so-called numerical chatter.

2. Rigid Constraint

The systems under consideration are presented schematically in Fig. 1. The first step in simulation of vertical motion of the rolling body of the system in Fig. 1a is to determine the constraint $y_C^k(x)$ for the vertical motion of the mass centre C of the relevant rigid body. The constraint is named here the rigid constraint to emphasise the difference between a kinematical trajectory of the rigid body rolling on the rigid foundation and the 'real' trajectory $y_C(x)$ of the rolling mass having finite contact stiffness and pressed against the foundation with finite external force.

For some ideal irregularities, for instance the threshold described with the step function on the flat surface, the rigid constraint is easily derived from geometrical relationships. For irregularities of any assumed or measured profiles, numerical computations are necessary. The method for effective numerical determination of the rigid constraint is presented in detail in [2]. For easier understanding let us use a discrete description of the system motion and denote the current horizontal position of the rolling mass centre C at time t_i by x_{Ci} and the

current point of contact by $D_i(x_{Di}, y_{Di})$ (see Fig. 2). On the line $x = x_{Di}$ a gap between the body and its foundation of irregular profile $y_r(x)$ equals 0, and the sum of $y_r(x)$ and a half of the vertical chord on the line has the maximum value. In the most general case, when nothing is assumed about the amplitudes of irregularities, the contact point must be searched for in the widest range, namely $x_{Di} \in (x_{Ci} - R, x_{Ci} + R)$.

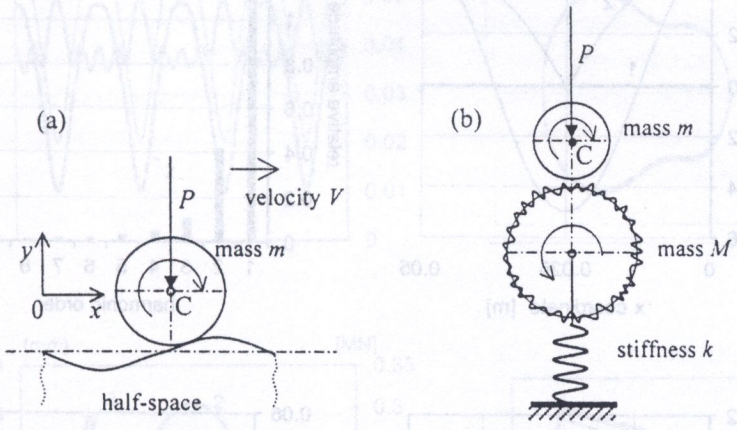

FIG. 1. Schemes of the systems under consideration: (a) wheel rolling on the irregular surface of a half-space; (b) wheel rolling on the irregular surface of compliant foundation represented by the effective mass M and the effective stiffness k.

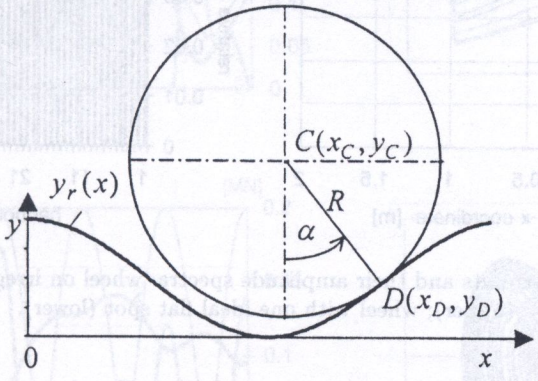

FIG. 2. Geometry of contact between a circle of radius R and an irregular profile $y_r(x)$.

Therefore, in order to determine the contact point and the constraint point a one-dimensional minimization problem has to be solved. Let us denote the decision variable by p. The problem can be formulated as follows:

$$p = x_{Di} \;\Rightarrow\; \sqrt{R^2 - (p - x_{Ci})^2} + y_r(p) = \max. \tag{2.1}$$

In the external coordinate system, the origin of which is moved to the mass centre, in the case when $y_r(x) \equiv 0$, we get

$$y_C^k(x_{Ci}) = \sqrt{R^2 - (x_{Di} - x_{Ci})^2} + y_r(x_{Di}) - R. \tag{2.2}$$

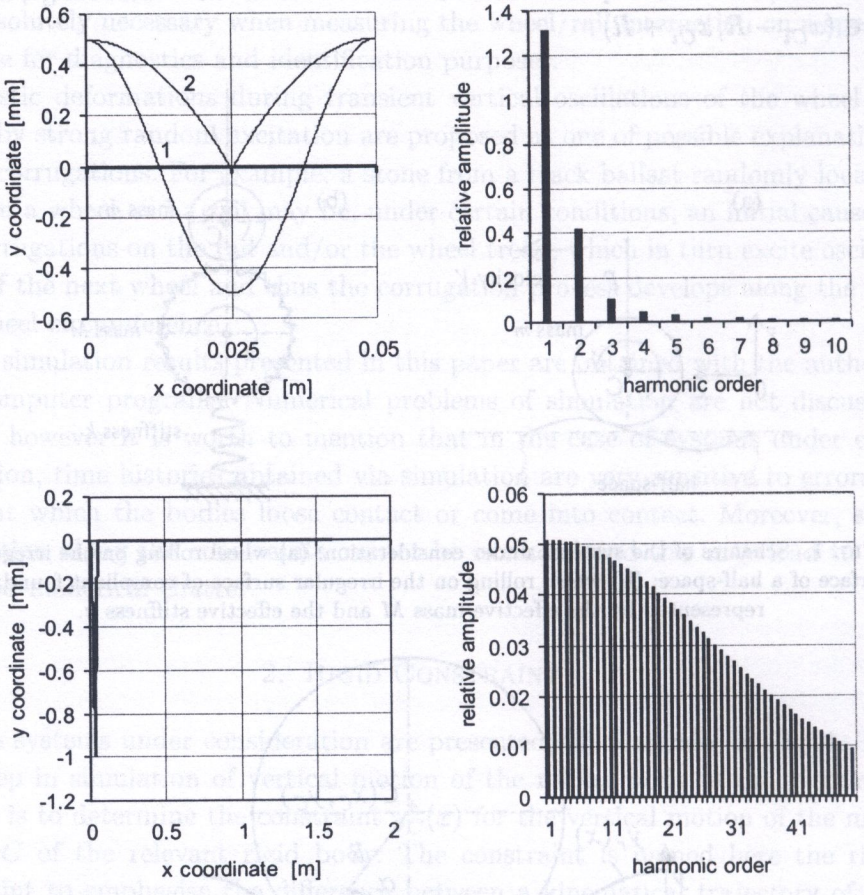

FIG. 3. Rigid constraints and their amplitude spectra: wheel on irregular cosine surface (upper); wheel with one ideal flat spot (lower).

Figure 3 shows the rigid constraints and their Fourier analysis for two cases of rolling motion: 1) an ideally round-shaped wheel rolling on an irregular surface of a cosine waveform; 2) a wheel with an ideal flat spot on its tread rolling on an even surface. The wheel with ideal flat means a wheel with a segment of a very short chord cut off. The ideal flat spot is a model of a real flat spot, caused by wheel slide, usually in consequence of overbraking under poor adhesive conditions. Severe flats have been known to derail a train. The flat spot

causes a tapping sound as the wheel rotates and it can usually be removed only by expensive reprofiling of the wheel on a lathe. The reference amplitude for the amplitudes of harmonic components is 0.1 mm in the case of cosine rail irregularity, and 1 mm in the case of flat spot.

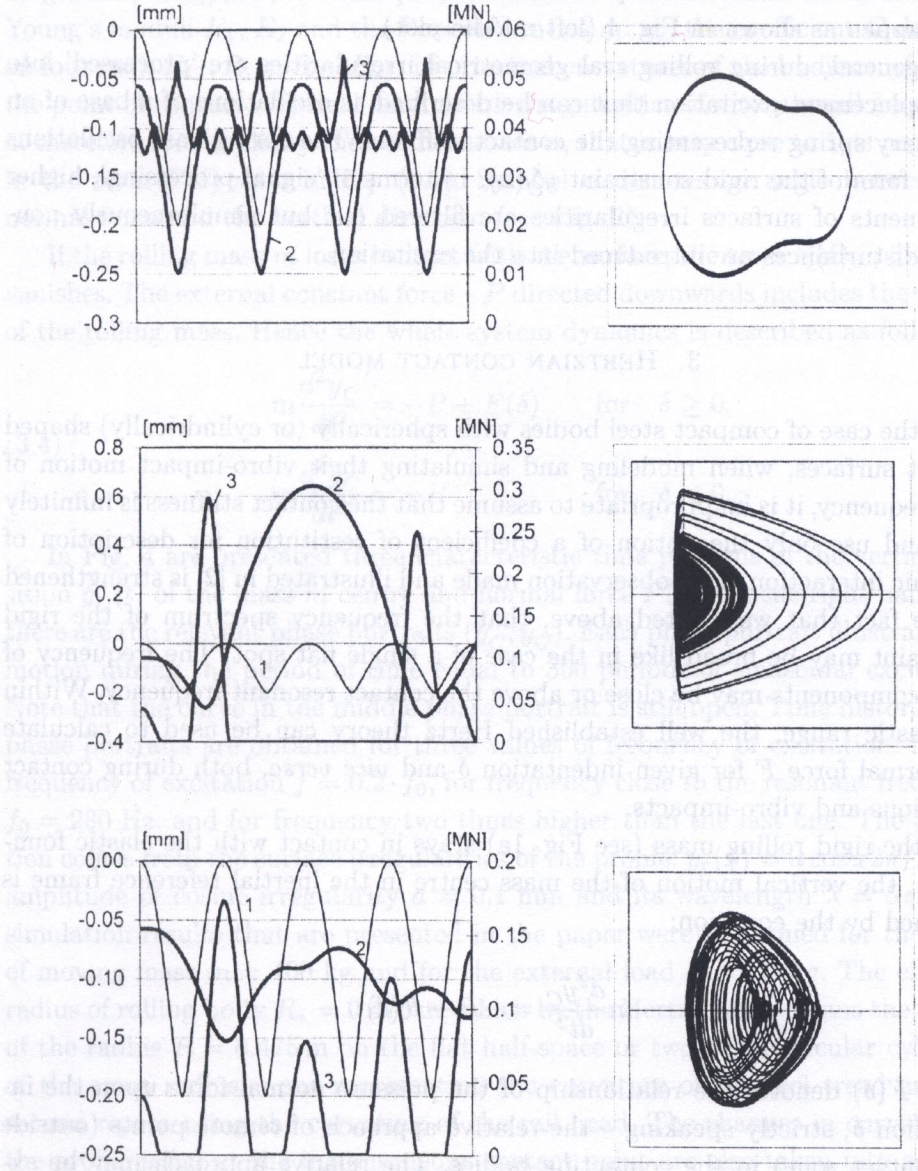

FIG. 4. Characteristic time patterns (left) and phase portraits (right) for the system of Fig. 1a: (a) – below resonance: $f = 0.2 \cdot f_0$; (b) – at resonance: $f_0 = 280$ Hz; (c) – above resonance: $f = 2 \cdot f_0$. *Lines indications:* 1 – rigid constraint, 2 – vertical position of the wheel centre.

Note in Fig. 3 that the rigid constraint $y_C^k(x)$ resulting from a single flat spot on the wheel circumference has a broad frequency spectrum. The 10th harmonic of the wheel rotational frequency has still a significant amplitude. The presence of high components in the spectrum increases the possibility of contact resonance at moderate train speeds. At contact resonance, high wheel bouncing may happen as shown in Fig. 4 (left middle plot).

In general, during rolling real geometrical irregularities are 'processed' into the displacement excitation that can be described as oscillations of a base of an imaginary spring representing the contact stiffness. The spring base oscillations have a form of the rigid constraint $y_C^k(x)$. In terms of 'signal processing', higher components of surfaces irregularities are filtered out but simultaneously nonlinear disturbances are introduced into the excitation.

3. Hertzian contact model

In the case of compact steel bodies with spherically (or cylindrically) shaped contact surfaces, when modeling and simulating their vibro-impact motion of high frequency, it is inappropriate to assume that the contact stiffness is infinitely high and use only the notion of a coefficient of restitution for description of dynamic interaction. This observation made and illustrated in [2] is strengthened by the fact that was stated above, that the frequency spectrum of the rigid constraint may be broad like in the case of a single flat spot. The frequency of many components may be close or above the contact resonant frequency. Within the elastic range, the well established Hertz theory can be used to calculate the normal force F for given indentation δ and *vice versa*, both during contact vibrations and vibro-impacts.

If the rigid rolling mass (see Fig. 1a) stays in contact with the elastic foundation, the vertical motion of the mass centre in the inertial reference frame is governed by the equation:

$$m\frac{d^2y_C}{dt^2} = -P + F(\delta), \tag{3.1}$$

where $F(\delta)$ denotes the relationship of the pressure normal force upon the indentation δ, strictly speaking – the relative approach of remote points (outside the contact zone) in the contacting bodies. The relative approach may be expressed as

$$\delta = -y_C + y_C^k. \tag{3.2}$$

In accordance with the Hertz theory, the relationship between the normal force F and the indentation has the form:

$$F(\delta) = C(E_1, E_2, \eta_1, \eta_2, R_{1I}, R_{1II}, R_{2I}, R_{2II})\delta^{3/2}. \tag{3.3}$$

In general, for given material properties of two bodies, that is for the given Young's moduli E_1, E_2 and the Poisson's ratios η_1, η_2, the coefficient C depends on four radii $R_{1I}, R_{1II}, R_{2I}, R_{2II}$ of principal curvatures of the bodies surfaces at the point of contact. We deal herein with irregularities of a very small amplitude a, therefore for simplicity the coefficient $\cos\alpha$, that is very close to 1, is neglected in the term $F(\delta)\cos\alpha$ in Eq. (2.1). Symbol α denotes an angle between the normal force and the vertical direction (see Fig. 2).

If the rolling mass m loses contact with the surface, the term $F(\delta)$ in Eq. (4.2) vanishes. The external constant force $-P$ directed downwards includes the weight of the rolling mass. Hence the whole system dynamics is described as follows:

$$\begin{aligned} m\frac{d^2y_C}{dt^2} &= -P + F(\delta) \qquad \text{for} \quad \delta \geq 0, \\ m\frac{d^2y_C}{dt^2} &= -P \qquad\qquad\quad \text{for} \quad \delta < 0. \end{aligned} \tag{3.4}$$

In Fig. 4 are presented three characteristic time patterns of the vertical position $y_C(t)$ of the mass m centre and normal force $F(t)$. On the right-hand side there are the relevant phase portraits $(y_C, \dot{y}_C)$. Each phase portrait illustrates the motion during the period of time equal to 300 periods of sinusoidal excitation. Note that the curve in the middle phase portrait is still open. Time histories and phase portraits are obtained for three values of frequency of excitation: for low frequency of excitation $f = 0.2 \cdot f_0$, for frequency close to the resonant frequency $f_0 = 280$ Hz, and for frequency two times higher than the last one. The excitation comes from the surface irregularities of the profile: $y_r(x) = a\cos x 2\pi/\lambda$. The amplitude of cosine irregularity $a = 0.1$ mm and its wavelength $\lambda = 5$ cm. All simulation results that are presented in the paper were performed for the value of moving mass $m = 400$ kg and for the external load $P = 10\,mg$. The effective radius of rolling body $R_* = 0.475$ m, which by the Hertz theory means the sphere of the radius $R = 0.475$ m on the flat half-space or two perpendicular cylinders of the same radius – one representing the curvature of a wheel tread and the second representing the curvature of the rail head. The changes in curvature of the profile $y_r(x)$ at the instantaneous contact point are also taken into account in the simulation algorithm.

Below the resonance the indentation δ is positive all the time, the rolling mass stays in contact with the foundation. The normal force F differs slightly

from the external load P. In the region of contact resonance (see middle plots), characteristic high bounces of the rolling mass m on the irregular surface of elastic foundation are observed. The maximum values of the normal force are several times greater than the external load. At frequencies much higher than the resonant frequency (see the bottom plots), the rolling mass is too 'heavy' or inert to follow fast vertical excitation, so it rolls over the tops of rail profile and loses periodically contact with the rail. The maximum normal forces are less than those at resonance, but much higher than below the resonance.

4. Johnson's model for contained plastic deformation

Using the Hertz theory of the normal contact in the analysis of elastic rolling contact is generally accepted. This is because the relationship $F(\delta)$ doesn't depend on the history of loading. In other words, loading through rolling ends with the same relationship $F(\delta)$ as normal loading or unloading. The situation is different in the analysis of elastic-plastic deformations. There are not generally accepted analytical models of normal elastic-plastic contact, both during normal loading/unloading and during loading by rolling. Therefore two different models were assumed, in a sense two extreme models, in order to grasp at least the main possible features of vertical vibro-impact motion superimposed on fast independent rolling.

Johnson's model concerns the normal contact of spherical bodies. Here the model was applied to the cylinders of the same radius having perpendicular axes. The rolling cylinder represents a wheel and the second one represents the rail head. So the Johnson model application was arbitrarily extended, however there is a premise to do that. By the Hertzian theory, the stress and deformations distribution within the contact zone for two perpendicular cylinders of radius R is the same as for a sphere in contact with the half-space.

The basic assumptions, which determine the contact zone stiffness in Johnson's cavity model of solid bodies contact, are as follows. Contact surface is encased in a hemi-spherical 'core'. Within the core there is a hydrostatic component of stress $\bar{p}$. Outside the core the stresses and displacements have radial symmetry and are the same as in an infinite elastic, perfectly-plastic body which contains a hemi-spherical cavity under a pressure $\bar{p}$. The displaced material does not pile-up around the contact area, it is accommodated by an elastic expansion of the surrounding hinterland. At the maximum indentation δ_c the effective radius R_* becomes larger. The unloading of the indenter is entirely elastic and proceeds according to the Hertz theory. Starting from the above assumptions, the analytical relationships between the normal force and the indentation were

derived [6, 7]. Figure 5 shows the relationship $F(\delta)$ in the range $\langle 0,\ 2\delta_Y\rangle$ during loading and force-indentation curve during unloading for the exemplary value of maximum indentation $\delta_c = 2\delta_Y$. The relevant analytical relationship during loading is given in the form:

$$F(\delta) = F_Y(2\delta/\delta_Y - 1)[1 + (3\vartheta_Y)^{-1}\ln(2\delta/\delta_Y - 1)]. \tag{4.1}$$

The values of the coefficient ϑ_Y differs slightly for different yield criterions. For the von Mises yield criterion the coefficient $\vartheta_Y = 1.1$. By the Hertz theory and von Mises yield criterion, the limiting normal force for elastic deformation F_Y has the form [7]:

$$F_Y = (3\pi/4)^2\,\vartheta_Y Y R_*^2(\vartheta_Y Y/E_*)^2. \tag{4.2}$$

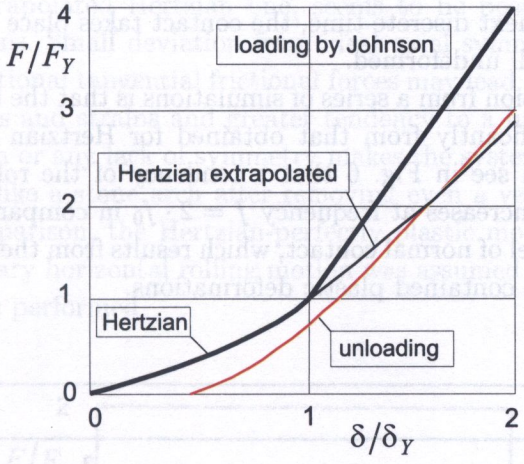

FIG. 5. Static force-indentation characteristics of normal contact.

In the case under consideration, the effective modulus $E_* = E_1 = E_2 = 2.14 \cdot 10^{11}\mathrm{N/m^2}$ and the effective radius $R_* = R_{1I} = R_{2II} = 0.475$ m, whereas R_{1I} is the radius of a rolling cylinder (wheel) and R_{2II} denotes the radius of non-moving perpendicular cylinder, or the radius of the rail head. Note that the limiting force F_Y is proportional to the uniaxial yield stress Y cubed.

For instantaneous values of dynamic normal force, which under normal operational conditions equals $1 \div 4$ times its static value (comp. Fig. 4), the difference between the extrapolated Hertzian characteristic and the Johnson's cavity model are small, both during loading and unloading (see Fig. 5). The final indentation is also relatively small. For maximum indentation $\delta_c = 2\delta_Y$ (and $F = 4 \cdot F_Y$), the final indentation $\delta_f = 0.27\delta_Y$.

Simulation of rolling contact was performed by using only the upper part of force-indentation characteristics, denoted in Fig. 5 as "loading by Johnson". Unlike similar vibro-impact systems without simultaneous rolling, the resultant normal force which influences the vertical motion of the rolling mass does not depend on the sign of the first derivative of the relative approach $\dot{\delta}$. This assumption is equivalent to the following one: the complex stress distribution which contributes to the resultant force in the contact zone is determined by the fast rolling process during which the contact zone is generally loaded; the stress distribution depends on relative approach of the bodies and does not depend on the direction of changes in the approach, because both the displacement and velocities in y-direction are much less than those in x-direction. Moreover, one of the Johnson's model features was neglected, that is a change of the effective radius R_* at the maximum indentation δ_c. The mass continues fast independent rolling and at the next discrete time, the contact takes place at the point where the surfaces are still undeformed.

General conclusion from a series of simulations is that the basic time patterns do not differ significantly from that obtained for Hertzian contact and given in Fig. 4. One can see in Fig. 6 that a tendency of the rolling mass towards bouncing slightly increases at frequency $f = 2 \cdot f_0$ in comparison to the system with Hertzian model of normal contact, which results from the increase of contact stiffness due to the contained plastic deformations.

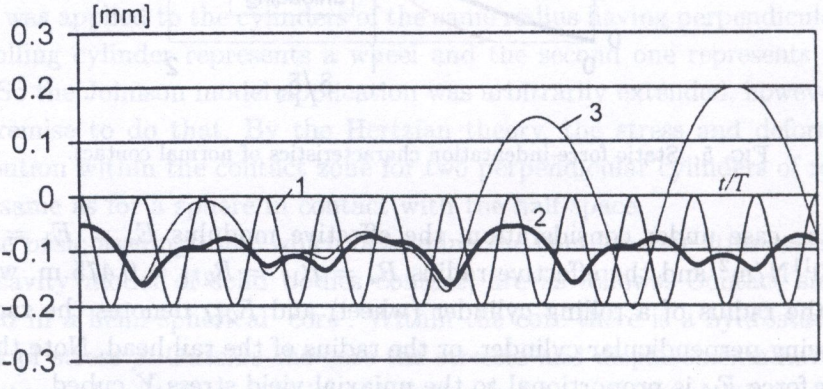

FIG. 6. Comparison of vibro-impacts forced by surface irreglarities at frequency $f = 2 \cdot f_0$. *Lines indications:* 1 – rigid constraint; 2 – vertical position of the rolling mass centre for Hertzian model, 3 – vertical position of the rolling mass centre for Johnson's model.

Different results were obtained for the system of the mass m lying on oscillating platform, in other words for immobile contact point (in the internal reference

frames fixed to the bodies). In such a system, large change of effective contact radius R_* at maximum indentation plays a significant role and makes the contact zone much stiffer within some permanently deformed area. Hysteresis damping resulting from successive loading and unloading at the same contact point depends very much on maximum indentation δ_c but in general is significant as well.

5. Hertzian–perfectly plastic model of contact

The Johnson's cavity model of elastic-plastic (contained) contact was derived for a static system of smooth spheres. The specific, ideally axially symmetrical distribution of stresses and deformations, which results in a stiffer contact zone than the extrapolated Hertzian one, seems to be possible in laboratory and static conditions. Small deviation from ideal axial symmetry, flash surface temperatures, additional tangential frictional forces may lead to less uniform distribution of stresses and strains and greater tendency to a full flow. In general, stress concentration or any lack of symmetry makes the system under load more prone to collapse, like a stone arch after removing even a very small fragment. Therefore, for comparison, the Hertzian-perfectly plastic model of normal contact during stationary horizontal rolling motion was assumed (see Fig. 7). Series of simulations were performed.

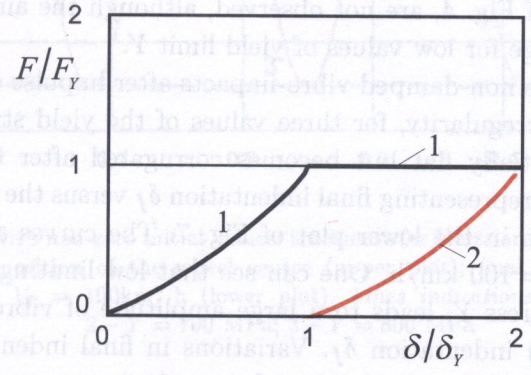

Fig. 7. Hertzian-perfectly plastic model of normal contact during stationary rolling motion: 1 – loading characteristic, 2 – unloading characteristics for maximum indentation $\delta_c = 2\delta_Y$.

The two sections of curve 1 in Fig. 7 was used to simulate the vertical motion of the rolling mass governed by the Eq. (5.1). The relationship $F(\delta)$ in equations

of motion (5.1) has the form:

$$
\begin{aligned}
F(\delta) &= C\delta^{3/2} \qquad \text{for} \qquad \delta \leq \delta_Y, \\
F(\delta) &= F_Y \qquad\quad \text{for} \qquad \delta > \delta_Y.
\end{aligned}
\tag{5.1}
$$

Curve 2 in Fig.7 is used for computation of a permanent regular pattern $y_f(x)$ left behind the rolling mass on the rail of the initial profile $y_r(x)$. In general,

$$
y_f(x) = y_r(x) - \delta_f(x) = y_r(x) - (\delta_c(x) - \delta_r(x)). \tag{5.2}
$$

For the initial profile $y_r(x) = 0$ and for the adopted model of contact, where the change in indentation δ_r as a result of ultimate elastic unloading does not depend on maximum indentation δ_c and is determined by relationship (3.3), the final pattern was computed by the rules:

$$
\begin{aligned}
y_f(x) &= 0 \qquad\qquad\quad \text{for} \qquad \delta(x) \leq \delta_Y, \\
y_f(x) &= -\delta(x) + (F_Y/C)^{2/3} \qquad \text{for} \qquad \delta(x) < \delta_Y.
\end{aligned}
\tag{5.3}
$$

Under the asumption of independent rolling $x_C = V_t\, t$; in discrete terms $x_{Ci} = V_t\, t_i$.

The main conclusion from the series of simulations of vibro-impacts forced by surface irregularities is as follows. At frequencies near the resonant frequency of the elastic system, characteristic high bounces of the rolling body, like in the middle plot of Fig. 4, are not observed, although the amplitudes of contact vibrations are large for low values of yield limit Y.

Figure 8 shows non-damped vibro-impacts after impulse excitation, e.g. with a single surface irregularity, for three values of the yield stress Y. In this case the surface is initially flat but becomes corrugated after the first run of the mass. The curves representing final indentation δ_f versus the x-coordinate (along the rail) are given in the lower plot of Fig. 7. The curves are obtained for the rolling speed $V_t = 100$ km/h. One can see that low limiting force F_Y, resulting from low yield stress Y, leads to a large amplitude of vibro-impacts and large final (permanent) indentation δ_f. Variations in final indentation $\delta_f(t)$ leave a permanent periodic pattern: $\delta_f(x) = \delta_f(x = V_t\, t)$ on a previously flat surface. Thus, excessive transient vibro-impacts during simultaneous rolling motion may be the initial cause of rail and wheel corrugations.

The distance between two subsequent ridges increases with the external constant load which is in accordance with the statement: "It (rail corrugations – author's note) typically consists of repeated shiny ridges and dark hollows on

the railhead (spaced approximately 30 to 80 mm apart along the rail in high-speed track, but at longer wavelengths in heavy-haul track)" [1].

The oscillations in Fig. 8a are not damped. This kind of oscillations may be classified as self-sustained. Physically it can be explained as follows. Independently of how large the maximum indentation is, due to concurrent independent rolling the mass is lifted back above the surface, provided the external force $P < F_Y$.

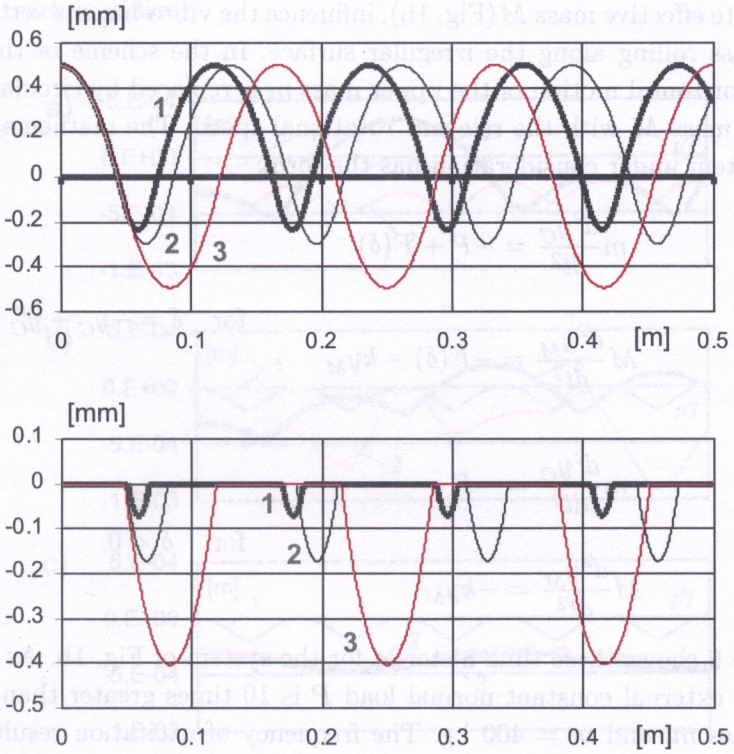

FIG. 8. Oscillations with non-zero initial values: transients for Hertzian-perfectly plastic model of contact: vertical position of the wheel centre (upper plot); final indentation along the rail at rolling speed V_t = 100km/ h (lower plot). *Lines indications*: 1 – Y = 600 MPa; 2 – Y = 700 MPa; 3 – Y = 800 MPa

6. SOFT FOUNDATION OF SMALL DYNAMIC INERTIA VERSUS STIFF FOUNDATION

So far the studies were focused on properties of the isolated system (Fig. 1a) consisting of the mass m and its foundation with an irregular surface. The system

may interact with neighbouring dynamic structures like the rolling mass suspension or the support structure of continuous elastic (or elastic-plastic) foundation of the rolling mass. In the case of the wheel/rail system the very soft primary suspension of the wheel (unsprung mass m), in comparison to the contact stiffness, can be neglected in the analysis of the system response to excitation caused by short rail irregularities [2].

Now, we will consider how the properties of the compliant support structure, namely its finite stiffness k represented by the spring and the inertia represented by the finite effective mass M (Fig. 1b), influence the vibro-impact vertical motion of the mass rolling along the irregular surface. In the scheme of the model in Fig. 1b, horizontal motion of the upper mass m is replaced by circular motion of the lower mass M with the relevant rotational speed. The mathematical model of the system under consideration has the form:

$$\begin{aligned} m\frac{d^2y_C}{dt^2} &= -P + F(\delta) \\ & \qquad \text{for} \quad \delta = -y_C + y_C^k + y_M \geq 0, \\ M\frac{d^2y_M}{dt^2} &= -F(\delta) - ky_M \end{aligned} \tag{6.1}$$

$$\begin{aligned} m\frac{d^2y_C}{dt^2} &= -P \\ & \qquad \text{for} \quad \delta < 0. \\ M\frac{d^2y_M}{dt^2} &= -ky_M \end{aligned}$$

Figure 9 shows three time histories for the system of Fig. 1b. As in all other cases, the external constant normal load P is 10 times greater than the weight of the mass m, and $m = 400$ kg. The frequency of excitation resulting from a cosine irregularity is $f = 280$ Hz and is close to the frequency of the contact resonance. Time histories are obtained for three different values of effective mass M and the same static stiffness k which is about five times less than the stiffness of the contact zone.

For $M = 10 \cdot m$ the time pattern is very similar to the case of infinite mass M (compare Fig. 4, middle plots). For $M = m$ the tendency of the rolling mass to bounce high off the platform is not so strong as in the previous case. For $M = 0.25 \cdot m$ the mass m stays in contact with the mass M at any instant of time. In Fig. 8 line 1 represents the rigid constraint. Line 2 represents the sum of the rigid constraint and the vertical position of the mass M; the difference between line 2 and line 3 represents indentation δ. It is seen in Fig. 9c

that the indentation is positive all the time, so both masses stay in contact all the time.

The exemplary simulation results are consistent with an intuitive notion about dynamical properties of the system under consideration. The support structure which is in a static sense softer than the contact zone of two hard bodies and has low dynamic inertia, eliminates vibro-impact motion induced by surface irregularities. From this point of view, soft rail track would be better than stiff slab track. However, maintenance and control of properties of soft traditional track is difficult.

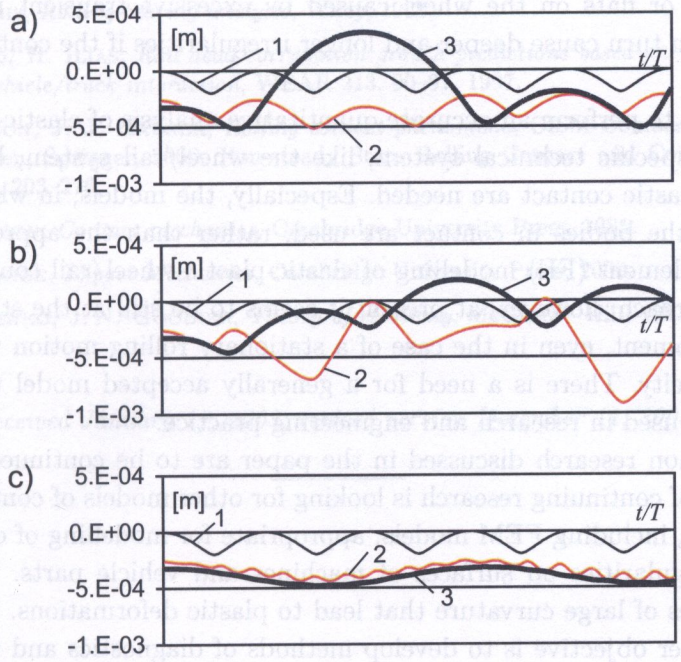

FIG. 9. Oscillations of the system in Fig. 1b at frequency close to the contact resonant frequency of the system in Fig. 1a: (a) – for mass $M = 10 \cdot m$; (b) – for mass $M = m$; (c) – for mass $M = 0.25 \cdot m$. *Lines indications:* 1 – rigid constraint; 2 – rigid constraint plus the vertical position of the point of mass M outside the contactzone; 3 – vertical position of the wheel centre.

7. CONCLUDING REMARKS AND THE OUTLOOK

In addition to the specific observations made so far, two more general conclusions are considered to be important to emphasize.

In the case of heavily loaded bodies, with respect to the yield limit, normal contact vibrations of a rolling body excited by a random single irregularity may start permanent deformations in the form of more or less periodic pattern along the previously flat surface. Though the material damping is low, and was neglected in the simulations, vertical vibrations vanish at last, but a permanent irregularity, as was previously remained, excites transient vibrations of the next wheel, and thus the corrugations may grow along the rolling surfaces. Certainly, frictional wear and plastic rolling decrease the roughness of irregularities but they cannot be entirely smoothed under normal operation conditions, if the initial permanent deformations are particularly large. A few initial successive hollows on the rail or flats on the wheel caused by excessive transient normal vibrations may in turn cause deeper and longer irregularities if the contact resonance takes place.

In order to perform an accurate quantitative analysis of elastic-plastic vibrations in a specific technical system, like the wheel/rail system, better models of elastic-plastic contact are needed. Especially, the models, in which the exact profiles of the bodies in contact are used, rather than the approximate ones. The finite element (FE) modelling of elastic-plastic wheel/rail contact, is surely a good approach; however, at present it seems to be still at the stage of studies and development, even in the case of a stationary rolling motion with constant rolling velocity. There is a need for a generally accepted model that could be confidently used in research and engineering practice.

Simulation research discussed in the paper are to be continued. One of the objectives of continuing research is looking for other models of contact of irregular surfaces, including FEM models, appropriate for modelling of excitation due to real irregularities on surfaces of machines and vehicle parts. In particular, irregularities of large curvature that lead to plastic deformations.

The other objective is to develop methods of diagnostics and identification, suitable for using in field tests on a special measuring section of the rail track. Speaking more precisely, the method for diagnostics of the wheelset faults and the method for estimating parameters of wheelsets and their suspensions, and for general assessing a potential of rail vehicles to damage the track. Identification and diagnostics in normal operation conditions is difficult due to high level of noise. The intent is to increase the distance between useful measuring signals and the noise by placing regular irregularities (sic) on the rail surfaces as a source of excitation of transient vibro-impacts that are used for diagnostics purposes. These irregularities introduced on purpose should have shape and dimensions so that they could be modelled accurately at the present stage of knowledge.

Acknowledgment

This work was partly supported by the Polish State Committee for Scientific Research (KBN Grant No. 5 T12 C019 24).

References

1. Bharat Bhushan, *Modern tribology handbook*, Vols. I, II, Chap, 34, Tribology of Rail Transport, CRC Press LLC, 2001.
2. R. Bogacz, Z. Kowalska, *Computer simulation of interaction between a wheel and corrugated rail*, European Journal of Mechanics A/Solids 20, 673–684, 2001.
3. T. A. Harris, *Rolling bearing analysis*, Wiley, 1966.
4. A. Igeland, H. Ilias, *Rail head corrugation growth predictions based on nonlinear high frequency vehicle/track interaction*, WEAR 213, 90–97, 1997.
5. Bo Jacobson, J. J. Kalker, *Rolling contact phenomena*, CISM Courses and Lectures No 411, Wien, Springer, 2000. Non-steady State Rolling Contact and Corrugations (by K. Knothe), 203–276.
6. K. L. Johnson, *Contact mechanics*, Cambridge University Press, 1985.
7. W. J. Stronge, *Impact Mechanics*, Cambridge University Press, 2000.
8. S. Timoshenko, J. N. Goodier, *Theory of elasticity*, McGraw – Hill, 1951.

Received January 17, 2003; revised version December 11, 2003.